POLITECNICO DI TORINO
Repository ISTITUZIONALE

Pendulum vibration absorbers with spatially-varying tangential friction: modelling and design

(Article begins on next page)

02 May 2024

PENDULUM VIBRATION ABSORBERS WITH SPATIALLY-VARYING TANGENTIAL FRICTION: MODELLING AND DESIGN

Emiliano Matta[1]

[1] Politecnico di Torino, Department of Architecture and Design
Viale Mattioli 39, 10125 Turin, Italy
e-mail: emiliano.matta@polito.it

Abstract

Passive vibration absorbers are widely used in structural control. They usually consist in a single-degree-of-freedom appendage of the main structure, tuned to a selected structural target mode by means of frequency and damping optimization. A classical configuration is the pendulum type, whose mass is bilaterally constrained along a curved trajectory and is typically connected to the structure through viscous dashpots. Although the principle is well known, the search for improved arrangements is still under way. In recent years this investigation has inspired a new type of bidirectional pendulum absorber (BPA), consisting of a mass moving along an optimal three-dimensional (3D) concave-up surface. For the BPA, the surface principal curvatures are conceived to ensure a bidirectional tuning to both principal modes of the structure, while damping is provided either by horizontal viscous dashpots or by vertical friction dampers between the BPA and the structure. In this paper, a BPA variant is proposed, in which damping is produced by the variable tangential friction force developing between the pendulum mass and the 3D surface, because of a spatially-varying friction coefficient. In fact, a friction coefficient pattern is proposed that varies along the pendulum surface proportionally to the modulus of the surface gradient. With this assumption, the absorber dissipative model proves nonlinear homogeneous at low response amplitudes. The resulting homogeneous BPA (HBPA) has a fundamental advantage over conventional friction-type absorbers, in that its equivalent damping ratio is independent of the amplitude of oscillations, i.e. its optimal performance is independent of the excitation level. At the same time, the HBPA is more compact and simpler than viscously damped BPAs, not requiring the installation of dampers. This paper presents the analytical modelling framework of the HBPA and a method for its optimal design. Numerical simulations under wind and earthquake loads are reported to compare the HBPA with classical viscously damped BPAs. Finally, the HBPA proves a promising alternative to existing pendulum absorbers, and the homogeneous tangential friction proves an effective way to realize amplitude-independent damping in structural systems.

Keywords: Amplitude-independent Damping, Homogeneous Friction, Pendulum Nonlinear Dynamics, Structural Control, Vibration Resonant Absorbers.

1 INTRODUCTION

Passive vibration absorbers are widely used in controlling civil engineering structures. Currently, they consist of single-degree-of-freedom (SDOF) appendages, tuned to the target structural mode through frequency and damping optimization [1-5]. One classical scheme is the pendulum absorber (PA), that exploits gravity to produce the restoring force, and consists of a damped mass moving along an arched trajectory. A PA can be conceived either as a hanging pendulum, suspended through cables or bars, or a supported pendulum, rolling or sliding on a physical track. In recent years, supported PAs have found several applications, because of their compactness, durability and versatility. Classical examples are the ball pendulum [6], the rolling and sliding pendulums [7], and the rocking pendulum.

Despite the numerous implementations reported in the literature and realized in practice, the research for novel arrangements is still ongoing, resulting in several new configurations, including the unbalanced rolling PA [8], the multiple-ball PA [9], and several types of track nonlinear energy sinks [10]. Among the others, this research has recently inspired the proposal of the so-called bidirectional pendulum absorber (BPA), made of a mass moving along an optimal three-dimensional (3D) concave surface, whose principal curvatures are chosen to ensure a bidirectional tuning to both principal modes of the main structure. The BPA has been proposed in two variants, respectively belonging to the supported pendulum and to the hanging pendulum types. The first variant is represented by the rolling-pendulum absorber proposed in [11]. Its 3D surface is manufactured as a double 3D rolling-pendulum bearing, comprising two equal concavities between which a rolling ball is interposed. Modifying the shape of the two concavities and the ball radius generates any possible 3D surface. The second variant is represented by the hanging-pendulum absorber proposed in [12]. Its 3D surface is realized through a Y-shaped configuration of the suspending cables. Modifying the length of the cables realizes any possible toroidal surface. In the first variant, energy dissipation is provided by horizontal viscous dampers, in the second variant it is provided by a vertical friction damper. In this latter case, the orthogonality between the damper and the 3D surface ensures an amplitude-independent equivalent damping, which should make the two variants approximately equivalent in terms of vibration suppression capability.

In this work, a further alternative of BPA is presented, in which damping is produced by the variable tangential friction developing between the pendulum mass and the 3D surface, as a result of a spatially-varying friction coefficient law [13, 14]. Namely, the friction coefficient is assumed to vary along the surface in proportion to the modulus of the surface gradient. This ensures a dissipative model which is nonlinear homogeneous at low response amplitudes [15]. Such a homogeneous BPA (HBPA) demonstrates superior to conventional friction ball absorbers (characterized by a constant friction coefficient), since its equivalent damping ratio proves amplitude independent, so that its performance does not vary with the excitation level. On the other hand, compared with the said existing BPAs ([11] and [12]), the HBPA is more compact, because it does not require the installation of additional dashpots. In the HBPA, friction is generated either by rolling [16] or by sliding, depending on the chosen type of pendulum. Friction can be spatially varied by changing the surface roughness or the material or the thickness of the surface coating, either continuously or discretely.

This paper describes the analytical model of the HBPA and presents an optimal methodology for its design. Simulations of single- and multi-story buildings under wind and seismic loads are reported, showing the pros and cons of the HBPA with respect to conventional viscously damped BPAs (VBPA) [17]. The results reveal that the HBPA is a promising alternative to conventional VBPAs, and that the homogeneous tangential friction is an effective solution to design mechanical systems having amplitude-independent damping.

2   GENERAL DESCRIPTION AND MODELING OF THE HBPA

2.1   Problem description

A BPA incorporating both viscous damping and tangential friction is shown in Fig. 1.
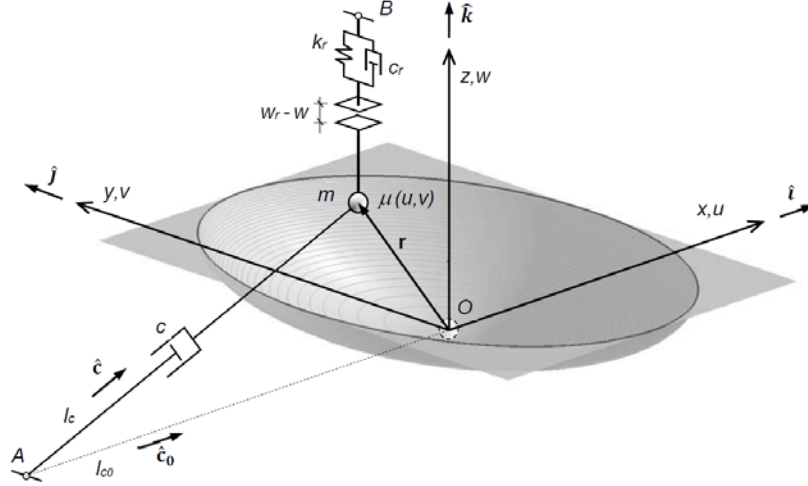

Figure 1: Schematic drawing of the BPA model.

Its model comprises a point mass m subject to gravity g and constrained to move along a 3D surface, connected to the structure at its minimum in O. The motion of m along the surface is opposed by: (i) the viscous damper linking m to the structure in A; (ii) the friction force acting on the surface; and (iii) the restrainer linking m to the structure in B. If structural rotations are negligible, the surface and the structural supports in A and B merely translate as the support in O. Denoting with u, v and w the coordinates of m w.r.t. the local reference system xyz fixed in O, and with $w = w(u,v) = w(\mathbf{q})$ the pendulum surface equation, the relative displacement of the HBPA w.r.t. the structure is $\mathbf{r} = [u,v,w]^T = [\mathbf{q}^T,w(\mathbf{q})]^T$, where u and v are the two independent coordinates, w is the dependent coordinate, and $\mathbf{q} = [u,v]^T$ is the HBPA degree-of-freedom vector. The structural support acceleration vector is $\mathbf{a} = [a_x,a_y,a_z]^T = [\mathbf{a}_h^T,a_z]^T$, and the BPA relative velocity vector is derived as $\dot{\mathbf{r}} = (\partial\mathbf{r}/\partial\mathbf{q})\dot{\mathbf{q}} = \mathbf{J}\dot{\mathbf{q}}$, where $\mathbf{J} = \partial\mathbf{r}/\partial\mathbf{q} = [\mathbf{I},\nabla w]^T$ is the Jacobian matrix of the kinematic transformation and $\nabla w = \partial w/\partial\mathbf{q}$ is the surface gradient.

2.2   The dissipative model

The model in Fig. 1 accounts for three different dissipative mechanisms: (i) one or more viscous dashpot; (ii) the tangential friction; and (iii) the fail-safe restrainer.

Assuming for brevity a single viscous dashpot with damping coefficient c, undeformed length l_{c0}, deformed length l_c, and undeformed and deformed coaxial versors $\hat{\mathbf{c}}_0$ and $\hat{\mathbf{c}}$, and denoting by $s_c = l_c - l_{c0}$ its axial elongation, the corresponding viscous force vector acting on m is $\mathbf{f}_c = -f_c\hat{\mathbf{c}}$, where $f_c = c\dot{s}_c$ and $\dot{s}_c = \hat{\mathbf{c}}^T\dot{\mathbf{r}} = \hat{\mathbf{c}}^T\mathbf{J}\dot{\mathbf{q}}$.

Assuming a dry friction coefficient varying along the pendulum surface according to an assigned law $\mu = \mu(u,v) = \mu(\mathbf{q})$, and denoting by N the modulus of the normal contact reaction force $\mathbf{N}$, the friction force can be expressed as $\mathbf{f}_\mu = -f_\mu\hat{\mathbf{t}}$, where $\hat{\mathbf{t}} = \dot{\mathbf{r}}/\|\dot{\mathbf{r}}\| = \mathbf{J}\dot{\mathbf{q}}/\sqrt{\dot{\mathbf{q}}^T\mathbf{J}^T\mathbf{J}\dot{\mathbf{q}}}$ is the tangent versor, and

$$f_\mu = \mu(\mathbf{q})N \tag{1}$$

In particular, the focus is here on a special friction pattern, where the friction coefficient varies along the pendulum surface proportionally to the surface gradient vector, according to:

$$\mu(\mathbf{q}) = \mu_0 \|\nabla w\| \tag{2}$$

where μ_0 is a proportionality factor, called the friction ratio. As shown later, Eq. (2) ensures a homogeneous first-order model.

Assuming a restrainer with stiffness k_r, damping coefficient c_r and initial clearance w_r, the restrainer force vector is $\mathbf{f}_r = -f_r\hat{\mathbf{k}}$, where $f_r = 0$ if $w \le w_r$ and $f_r = k_r(w - w_r) + c_r\dot{w}$ if $w > w_r$, with $\dot{w} = \nabla w^T \dot{\mathbf{q}}$.

The total dissipative force applied to m by the three mechanisms is therefore $\mathbf{f}_d = \mathbf{f}_c + \mathbf{f}_\mu + \mathbf{f}_r$. Denoting by $\mathbf{w} = -mg\hat{\mathbf{k}}$ the weight of m, and by $\lambda_d = m(\mathbf{a} + \ddot{\mathbf{r}})$ the dynamic interaction force between the BPA and its support, the dynamic equilibrium of m reads $\mathbf{w} + \mathbf{N} + \mathbf{f}_d = \lambda_d$, which finally provides N in Eq. (1) as the modulus of the vector $\mathbf{N} = \lambda_d - \mathbf{w} - \mathbf{f}_d$.

2.3 The nonlinear three-dimensional model of the BPA

The BPA dynamic equation can be obtained by applying the Euler-Lagrange equation to the mass m:

$$\frac{d}{dt}\left(\frac{\partial T}{\partial \dot{\mathbf{q}}}\right) - \frac{\partial T}{\partial \mathbf{q}} + \frac{\partial V_g}{\partial \mathbf{q}} + \mathbf{Q}_i + \mathbf{Q}_e = \mathbf{0} \tag{3}$$

where $T = m\dot{\mathbf{r}}^T\dot{\mathbf{r}}/2$ is the kinetic energy of m; $V_g = mgw$ is its gravitational potential energy; $\mathbf{Q}_i = -\mathbf{J}^T\mathbf{f}_d$ is the generalized internal force due to the total dissipative force $\mathbf{f}_d$; and $\mathbf{Q}_e = m\mathbf{J}^T\mathbf{a}$ is the generalized external force due to the support acceleration. Deriving the first three terms of Eq. (3), and denoting by $\mathbf{M}^q = m\mathbf{J}^T\mathbf{J}$ the BPA generalized mass matrix, the BPA fully nonlinear 3D model is finally obtained as

$$\mathbf{M}^q\ddot{\mathbf{q}} + \mathbf{Q}_i + mg\nabla w = -m\mathbf{J}^T\mathbf{a} - \left(\dot{\mathbf{M}}^q\dot{\mathbf{q}} - \frac{\partial T}{\partial \mathbf{q}}\right) \tag{4}$$

In Eq. (4), the dissipative term on the left-hand side can be expressed as

$$\mathbf{Q}_i = -\mathbf{J}^T\mathbf{f}_d = f_c\mathbf{J}^T\hat{\mathbf{c}} + f_\mu\mathbf{J}^T\hat{\mathbf{t}} + f_r\mathbf{J}^T\hat{\mathbf{k}} \tag{5}$$

where

$$f_c\mathbf{J}^T\hat{\mathbf{c}} = c\left(\mathbf{J}^T\hat{\mathbf{c}}\hat{\mathbf{c}}^T\mathbf{J}\right)\dot{\mathbf{q}} \tag{6}$$

$$f_\mu\mathbf{J}^T\hat{\mathbf{t}} = \mu(\mathbf{q})N\mathbf{J}^T\mathbf{J}\dot{\mathbf{q}}/\sqrt{\dot{\mathbf{q}}^T\mathbf{J}^T\mathbf{J}\dot{\mathbf{q}}} \tag{7}$$

$$f_r\mathbf{J}^T\hat{\mathbf{k}} = f_r\nabla w \tag{8}$$

are the generalized viscous, friction and restrainer force vectors, respectively.

2.4 The nonlinear three-dimensional model of the BPA-MDOF system

The dynamic equation of a linear multi-degree-of-freedom (MDOF) structure coupled with the BPA and subjected to external forces and ground accelerations is

$$\mathbf{M}_s\ddot{\mathbf{q}}_s + \mathbf{C}_s\dot{\mathbf{q}}_s + \mathbf{K}_s\mathbf{q}_s + \mathbf{L}^T\lambda_d = \mathbf{f}_s - \mathbf{M}_s\mathbf{R}_s\ddot{\mathbf{r}}_g \tag{9}$$

where $\mathbf{q}_s$ is the vector of structural DOFs; $\mathbf{M}_s$, $\mathbf{C}_s$ and $\mathbf{K}_s$ are the structural matrices of mass, damping and stiffness; $\mathbf{f}_s$ is the vector of external forces; $\ddot{\mathbf{r}}_g$ is the vector of ground accelerations; $\mathbf{L}$ and $\mathbf{R}_s$ are kinematic and topological matrices. Combining Eqs. (4) and (9), the fully nonlinear coupled dynamic equation can be finally expressed as

$$
\begin{bmatrix} \mathbf{M}_s + m\mathbf{L}^T\mathbf{L} & m\mathbf{L}^T\mathbf{J} \\ m\mathbf{J}^T\mathbf{L} & \mathbf{M}^q \end{bmatrix} \begin{bmatrix} \ddot{\mathbf{q}}_s \\ \ddot{\mathbf{q}} \end{bmatrix} + \begin{bmatrix} \mathbf{C}_s & \mathbf{0} \\ \mathbf{0} & \mathbf{0} \end{bmatrix} \begin{bmatrix} \dot{\mathbf{q}}_s \\ \dot{\mathbf{q}} \end{bmatrix} + \begin{bmatrix} \mathbf{K}_s & \mathbf{0} \\ \mathbf{0} & \mathbf{0} \end{bmatrix} \begin{bmatrix} \mathbf{q}_s \\ \mathbf{q} \end{bmatrix} +
$$
$$
+ \begin{bmatrix} \mathbf{0} \\ \mathbf{Q}_i \end{bmatrix} = \begin{bmatrix} \mathbf{f}_s \\ \mathbf{0} \end{bmatrix} - \begin{bmatrix} \mathbf{M}_s + m\mathbf{L}^T\mathbf{L} \\ m\mathbf{J}^T\mathbf{L} \end{bmatrix} \mathbf{R}_s\ddot{\mathbf{r}}_g - \begin{bmatrix} m\mathbf{L}^T\mathbf{J}\dot{\mathbf{q}} \\ \dot{\mathbf{M}}^q\dot{\mathbf{q}} - \dfrac{\partial T}{\partial \mathbf{q}} \end{bmatrix}.
\tag{10}
$$

2.5 The first-order approximated model

Some fundamental properties of the BPA can be demonstrated by considering its response at low amplitudes. By developing in Taylor series Eqs. (4) to (8), and by truncating higher-order terms, the first-order 3D model of the BPA is obtained as

$$
m\ddot{\mathbf{q}} + \mathbf{C}\dot{\mathbf{q}} + N_0\mathbf{K}_w\mathbf{q} + \mu_0 N_0 \|\mathbf{K}_w\mathbf{q}\| \dot{\mathbf{q}}/\|\dot{\mathbf{q}}\| = -m\mathbf{a}_h
\tag{11}
$$

where: $\mathbf{C}$ is the BPA viscous damping matrix, given by

$$
\mathbf{C} = c \begin{bmatrix} \hat{c}_{0x}^2 & \hat{c}_{0x}\hat{c}_{0y} \\ \hat{c}_{0x}\hat{c}_{0y} & \hat{c}_{0y}^2 \end{bmatrix}
\tag{12}
$$

if the viscous damper is set parallel to the xy plane; $N_0 = N/(mg) = 1+a_z/g$ is the normalized normal component of the reaction force; $\mathbf{a}_h = [a_x, a_y]^T$ is the vector of horizontal accelerations at the support; and $\mathbf{K}_w$ is the equivalent pendular stiffness matrix, given by:

$$
\mathbf{K}_w = \begin{bmatrix} k_{wx} & 0 \\ 0 & k_{wy} \end{bmatrix} = mg \begin{bmatrix} 1/L_x & 0 \\ 0 & 1/L_y \end{bmatrix} = mg\mathbf{H}_w
\tag{13}
$$

where $\mathbf{H}_w$ is the Hessian matrix of $w(\mathbf{q})$ in $\mathbf{0}$, and L_x and L_y are the pendulum lengths along x and y.

Accordingly, the first-order 3D model of the BPA-structure coupled system is

$$
\begin{bmatrix} \mathbf{M}_s + m\mathbf{L}_h^T\mathbf{L}_h & m\mathbf{L}_h^T \\ m\mathbf{L}_h & m\mathbf{I} \end{bmatrix} \begin{bmatrix} \ddot{\mathbf{q}}_s \\ \ddot{\mathbf{q}} \end{bmatrix} + \begin{bmatrix} \mathbf{C}_s & \mathbf{0} \\ \mathbf{0} & \mathbf{C} + \mu_0 N_0\|\mathbf{K}_w\mathbf{q}\|/\|\dot{\mathbf{q}}\| \end{bmatrix} \begin{bmatrix} \dot{\mathbf{q}}_s \\ \dot{\mathbf{q}} \end{bmatrix} +
$$
$$
+ \begin{bmatrix} \mathbf{K}_s & \mathbf{0} \\ \mathbf{0} & N_0\mathbf{K}_w \end{bmatrix} \begin{bmatrix} \mathbf{q}_s \\ \mathbf{q} \end{bmatrix} = \begin{bmatrix} \mathbf{f}_s \\ \mathbf{0} \end{bmatrix} - \begin{bmatrix} \mathbf{M}_s + m\mathbf{L}_h^T\mathbf{L}_h \\ m\mathbf{L}_h \end{bmatrix} \mathbf{R}_s\ddot{\mathbf{r}}_g,
\tag{14}
$$

where $\mathbf{L}_h$ is the vector containing the first two columns of $\mathbf{L}$.

Based on Eq. (11), the following observations can be formulated:

1) the inertia force $m\ddot{\mathbf{q}}$ and the restoring force $N_0\mathbf{K}_w\mathbf{q}$ are linear and uncoupled along x and y; this holds for the viscous force $\mathbf{C}\dot{\mathbf{q}}$, provided that all viscous dampers are aligned with the coordinate axes;

2) the friction force has modulus $\mu_0 N_0\|\mathbf{K}_w\mathbf{q}\|$ and has direction and sign of the tangent versor $\dot{\mathbf{q}}/\|\dot{\mathbf{q}}\|$; because its modulus, direction and sign are nonlinear and coupled, the friction force is a nonlinear coupled function of $\mathbf{q}$ and $\dot{\mathbf{q}}$;

3) because its modulus increases proportionally with $\mathbf{q}$ and does not depend on $\dot{\mathbf{q}}$, the friction force is a homogeneous function of $\mathbf{q}$ and $\dot{\mathbf{q}}$; Eq. (11) is therefore homogeneous and

its solution is proportional to $\mathbf{a}_h$, which definitely makes the HBPA a first-order nonlinear but homogeneous system.

2.6 The simplified two-dimensional model

The 3D first-order models in Eqs. (11) and (14) can be further simplified for design purposes, assuming that: (i) the motion occurs in a vertical coordinate plane, e.g. the xz plane, so the model becomes two-dimensional (2D); (ii) in the xz plane the structural target frequency is far from the other ones, so the MDOF structure can be reduced to a 1DOF mode-generalized system; (iii) the vertical acceleration input a_z is negligible, so $N_0 = 1$. Under these conditions, Eqs. (11) and (14) become respectively

$$m\ddot{u} + c_x\dot{u} + k_{wx}[1 + \mu_0\text{sign}(u\dot{u})]u = -ma_x \tag{15}$$

$$\begin{bmatrix} m_{sx} + m & m \\ m & m \end{bmatrix}\begin{bmatrix} \ddot{u}_s \\ \ddot{u} \end{bmatrix} + \begin{bmatrix} c_{sx} & 0 \\ 0 & c_x \end{bmatrix}\begin{bmatrix} \dot{u}_s \\ \dot{u} \end{bmatrix} +$$
$$+ \begin{bmatrix} k_{sx} & 0 \\ 0 & k_{wx}[1 + \mu_0\text{sign}(u\dot{u})] \end{bmatrix}\begin{bmatrix} u_s \\ u \end{bmatrix} = \begin{bmatrix} f_{sx} \\ 0 \end{bmatrix} - \begin{bmatrix} m_{sx} + m \\ m \end{bmatrix}\ddot{u}_g, \tag{16}$$

where u_s is the horizontal displacement of the structure w.r.t. the ground; m_{sx}, c_{sx} and k_{sx} are the generalized mass, damping and stiffness of the structure along x; and c_x is the BPA viscous damping coefficient along x.

Eqs. (15) and (16) can be finally recast in modal form as

$$\ddot{u} + 2\varsigma_x\omega_x\dot{u} + \omega_x^2[1 + \mu_0\text{sign}(u\dot{u})]u = -a_x \tag{17}$$

$$\begin{bmatrix} 1 + m_{Rx} & m_{Rx} \\ 1 & 1 \end{bmatrix}\begin{bmatrix} \ddot{u}_s \\ \ddot{u} \end{bmatrix} + 2\omega_{sx}\begin{bmatrix} \varsigma_{sx} & 0 \\ 0 & \varsigma_x\omega_{Rx} \end{bmatrix}\begin{bmatrix} \dot{u}_s \\ \dot{u} \end{bmatrix} +$$
$$+ \omega_{sx}^2\begin{bmatrix} 1 & 0 \\ 0 & \omega_{Rx}^2[1 + \mu_0\text{sign}(u\dot{u})] \end{bmatrix}\begin{bmatrix} u_s \\ u \end{bmatrix} = \begin{bmatrix} \bar{f}_{sx} \\ 0 \end{bmatrix} - \begin{bmatrix} 1 + m_{Rx} \\ 1 \end{bmatrix}\ddot{u}_g, \tag{18}$$

where $m_{Rx} = m/m_{sx}$ is the BPA mass ratio along x; $\omega_{sx} = \sqrt{k_{sx}/m_s}$ and $\omega_x = \sqrt{g/L_x}$ are the structure and BPA circular frequencies along x; $\omega_{Rx} = \omega_x/\omega_{sx}$ is the BPA frequency ratio along x; and $\varsigma_{sx} = c_{sx}/(2\omega_{sx}m_{sx})$ and $\varsigma_x = c_x/(2\omega_x m)$ are the structure and BPA viscous damping ratios along x.

3 THE DESIGN PROCEDURE

A design methodology is here presented for a BPA of either viscous type (VBPA) or homogeneous friction type (HBPA). Their models can be obtained from those derived in Section II, by respectively annulling the friction or the viscous terms. The methodology comprises two steps: (1) a 2D first-order optimization; and (2) a 3D second-order completion.

3.1 The two-dimensional first-order optimization

According to the simplified 2D model in Eq. (18), which admits an uncoupled motion along x and y, and assuming the structure known, both the VBPA and the HBPA are completely determined, in each direction, by three dimensionless design parameters: m_{Rx}, ω_{Rx} and ς_x for the VBPA, and m_{Rx}, ω_{Rx} and μ_0 for the HBPA. If the mass ratio m_{Rx} is fixed based on cost-benefit expectations, the two remaining free parameters can be obtained by solving an H∞ design problem [18], i.e. by minimizing the H∞ norm of a significant input-output transfer function (TF) of the structure-BPA system. Denoting by ω the circular frequency of the excitation in-

put, two possible TFs are here considered for each BPA type: the force-to-displacement transfer function $T_f(\omega)$ (significant for wind load applications), and the ground acceleration-to-displacement transfer function $T_g(\omega)$ (significant for seismic load applications). Denoting as the response ratio R_x the ratio between the controlled and the uncontrolled H_∞ norm of those TFs, optimization can be formalized as follows, respectively for a wind-oriented VBPA:

$$R_{xopt} = \min_{\omega_{Rx},\varsigma_x} R_x = \min_{\omega_{Rx},\varsigma_x} \max_\omega \left(\left|T_f(\omega)\right|^{con} \Big/ \left\|T_f\right\|_\infty^{unc} \right) \tag{19}$$

for a seismic-oriented VBPA:

$$R_{xopt} = \min_{\omega_{Rx},\varsigma_x} R_x = \min_{\omega_{Rx},\varsigma_x} \max_\omega \left(\left|T_g(\omega)\right|^{con} \Big/ \left\|T_g\right\|_\infty^{unc} \right) \tag{20}$$

for a wind-oriented HBPA:

$$R_{xopt} = \min_{\omega_{Rx},\mu_0} R_x = \min_{\omega_{Rx},\mu_0} \max_\omega \left(\left|T_f(\omega)\right|^{con} \Big/ \left\|T_f\right\|_\infty^{unc} \right) \tag{21}$$

and for a seismic-oriented HBPA:

$$R_{xopt} = \min_{\omega_{Rx},\mu_0} R_x = \min_{\omega_{Rx},\mu_0} \max_\omega \left(\left|T_g(\omega)\right|^{con} \Big/ \left\|T_g\right\|_\infty^{unc} \right) \tag{22}$$

Eqs. (19) and (20) give the optimal VBPA parameters ω_{Rxopt} and ς_{xopt}, respectively for wind and seismic control. Eqs. (21) and (22) give the optimal HBPA parameters ω_{Rxopt} and μ_{0opt}, respectively for wind and seismic control.

The min.max. problems in Eqs. (19) to (22) are here numerically solved using a branch & bound search algorithm analogue to the one used in [5], followed by a nonlinear least-square solver for improved local convergence. The computation of the VBPA TF in Eqs. (19) and (20) is straightforward, based on classical closed-form expressions available for linear mechanical models, whereas the computation of the HBPA TF in Eqs. (21) and (22) needs simulating the system response time-history at each input frequency until stabilization of the response amplitude.

Assuming a structural damping ratio $\zeta_{sx} = 2\%$, the optimization results are reported in Fig. 2 for the VBPA (dashed lines) and the HBPA (continuous lines), as a function of the mass ratio m_{Rx}. The wind-oriented optimization is reported on the left (subfigures a, c and e), while the seismic-oriented optimization is reported on the right (subfigures b, d and f). Subfigures a and b show the optimal frequency ratio; subfigures c and d show the optimal damping ratio (for the VBPA) and the optimal friction ratio (for the HBPA), this latter normalized to π; and subfigures e and f show the optimal response ratios. Whereas the results obtained for the VBPA are well known (see for instance [19]) and do not deserve specific comments, the results obtained for the HBPA reveal that the optimal HBPA slightly improves the VBPA performance, especially for large values of m_{Rx}. To achieve this, ω_{Rxopt} is always larger for the HBPA than for the VBPA, except for very small mass ratios, when the optimal frequency ratio converges to unity for both types. On the other hand, μ_{0opt} converges to $\pi \cdot \varsigma_{xopt}$ for small mass ratios, but tends to be increasingly smaller than $\pi \cdot \varsigma_{xopt}$ as the mass ratio increases. The same trends are appreciated for the wind-oriented and the seismic-oriented design types.

Assuming that the structural target modes have the same damping ratio and the same generalized mass in the two horizontal directions, the results obtained above hold along x and y, and the x subscript can be dropped for brevity. Together with the mass ratio m_R and with the structural parameters, the resulting optimal dimensionless parameters ω_{Ropt}, ς_{opt} and μ_{0opt} allow the computation of all BPA dimensional parameters involved in the low amplitude domain, i.e. the BPA mass m, the BPA circular frequencies ω_x and ω_y, the BPA pendulum

lengths L_x and L_y, the VBPA damping coefficients c_x and c_y, and the HBPA friction pattern around the origin, this latter given around by

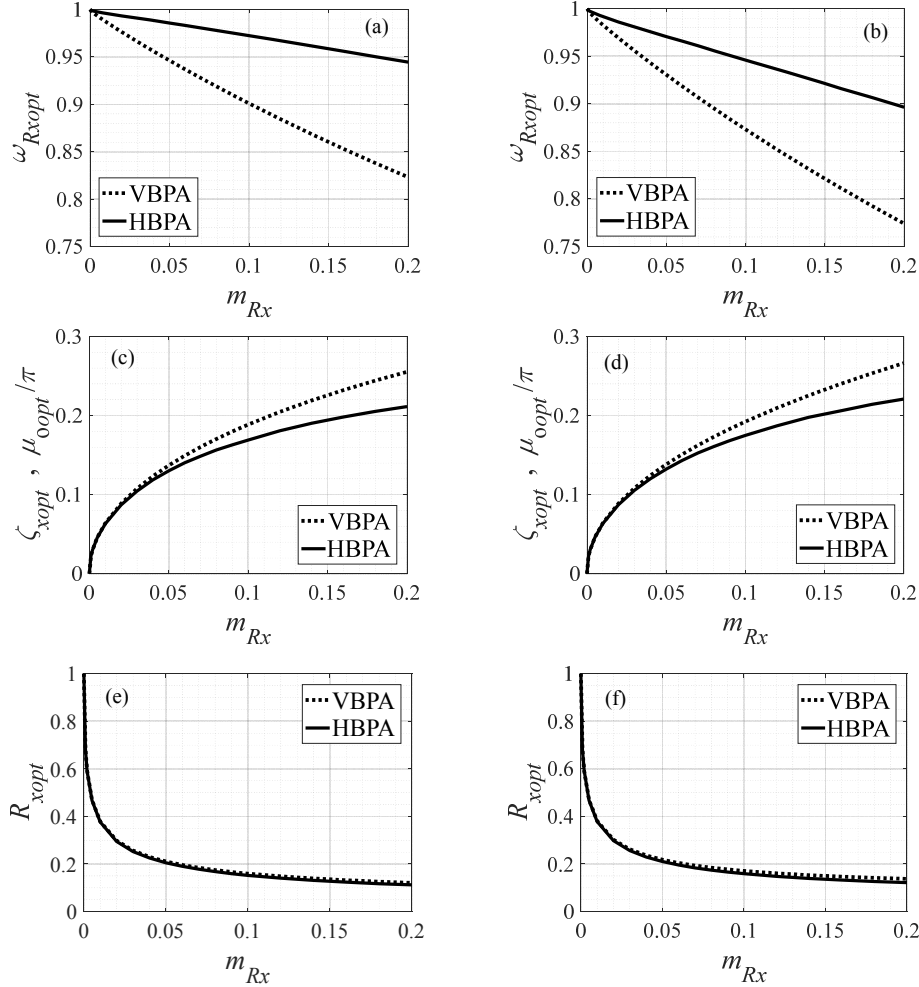$$\mu(\mathbf{q}) = \mu_{0opt} \| \nabla w \| \approx \mu_{0opt} \sqrt{u^2 / L_x^2 + v^2 / L_y^2} \qquad (23)$$

Figure 2: H_∞ optimal design of a VBPA (dotted lines) and a HBPA (continuous lines), as a function of m_{Rx}, for $\zeta_{sx} = 2\%$. Left: wind-oriented design. Right: seismic-oriented design. First row: optimal frequency ratios. Second row: optimal viscous/friction damping ratios. Third row: optimal response ratios.

3.2 The three-dimensional second-order completion

The subsequent completion step provides the BPA parameters which, involved only in the large-displacement domain, are excluded from the previous optimization step. These parameters include the pendulum shape (and consequently the friction pattern) far from the origin, the length and number of viscous dashpots, and the restrainer properties.

By providing L_x and L_y, the optimization step determines the pendulum shape around the origin. Far from it, however, different shapes correspond to the same pair of L_x and L_y. Among the possible choices are, for example, the ellipsoid, the torus or the elliptic paraboloid. If the ellipsoid is chosen, infinite ways of assigning its semi-axes b_x, b_y and b_z exist, all providing the desired L_x and L_y pair. Then, by imposing that $b_z = \sqrt{b_x b_y}$, only one admissible

ellipsoid exists, of semi-axes $b_x = \sqrt[4]{L_x^3 L_y}$, $b_y = \sqrt[4]{L_x L_y^3}$ and $b_z = \sqrt{L_x L_y}$. This choice is systematically assumed in the sequel.

With this assumption, the friction pattern defined by Eq. (2) becomes:

$$\mu(\mathbf{q}) = \mu_{0opt} \sqrt{\left(\frac{u^2}{L_x^2} + \frac{v^2}{L_y^2}\right) \bigg/ \left(1 - \frac{u^2}{b_x^2} - \frac{v^2}{b_y^2}\right)} \tag{24}$$

where $\mu(\mathbf{q})$ tends to zero around the origin, tends to infinite at the ellipsoid equator, and describes iso-friction curves intersecting the level curves, as shown in Fig. 3 for an ellipsoid having $L_y/L_x = 2$, truncated at $w_r = b_z/2$. Both Figs. 3 (a) and (b) represent nine level curves, uniformly spaced between 0 and w_r, and nine iso-friction curves, uniformly spaced between 0 and $2 \mu_{0opt}$.
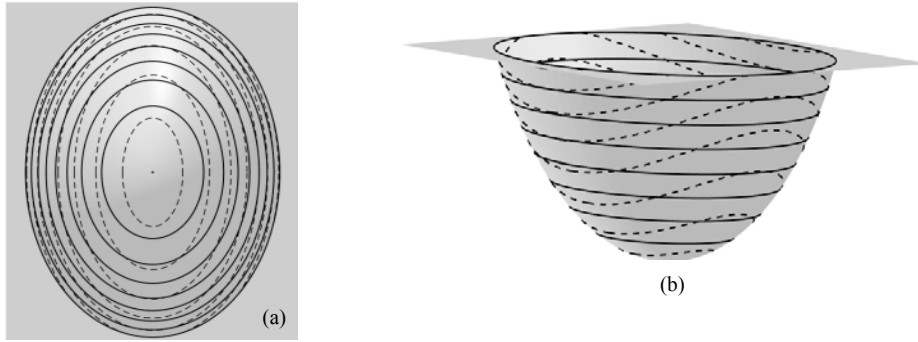

(a)

(b)

Figure 3: Level curves (continuous) and iso-friction curves (dashed) if $L_y/L_x = 2$: (a) planar view; (b) axonometric view (with the z dimension doubled for clarity).

Regarding the design of the viscous dampers, the optimization step provides the optimal values of c_x and c_y, in the assumption of a single damper for every direction. If more dampers are used in the same direction, the optimal damping coefficient must be subdivided among them. The length of the viscous dampers does not enter the optimization step. In the sequel, two dampers will be systematically assumed in each direction, each having length $l_{c0} = b_z = \sqrt{L_x L_y}$.

Finally, the restrainer too does not enter the optimization step. Its mechanical properties can be assigned to simulate a dissipative impact. In the remaining of this paper, its stiffness is systematically chosen as $k_r = m\omega_r^2$, where $\omega_r = 20\sqrt{\omega_x \omega_y}$; its damping is assigned as $c_r = 2\varsigma_r \omega_r m$, where $\varsigma_r = -\ln e_r \big/ \sqrt{\pi^2 + \ln^2 e_r}$ and $e_r = 0.5$ (elastic restitution coefficient); its clearance is assigned as $w_r = b_z/2$.

4 TWO-DIMENSIONAL SIMULATIONS OF THE FIRST-ORDER MODEL

The optimal VBPA and the optimal HBPA are here compared at low amplitudes, by assuming the first-order 2D models expressed by Eqs. (16) or (18). The structure is a 2% damped SDOF system.

4.1 White noise force excitation

Optimized according to the wind-oriented design procedure described in Section 3, the VBPA and the HBPA are compared by subjecting the SDOF structure to a stationary Gaussi-

an zero-mean white-noise force $\bar{f}_{sx}$. For the uncontrolled and for the VBPA-controlled structure (linear cases), the system stationary root-mean-square (rms) response is computed solving the Lyapunov equation [18]. For the HBPA-controlled structure, the rms response is computed through Monte Carlo simulations, using 100 realizations of the input process. Each realization has lasts $3600 T_{sx}$, with a sampling time of $0.01 T_{sx}$, T_{sx} being the structural period.

The BPA performance is evaluated in terms of the rms structural displacement, rms(u_s), and the rms BPA relative displacement (stroke), rms(u). Two performance indices are considered, computed dividing the controlled value of the rms responses by the uncontrolled value of the rms structural displacement: the displacement response ratios R_{dx} = rms(u_s)con/ rms(u_s)unc, and the stroke response ratio R_{sx} = rms(u)con/ rms(u_s)unc.

The two response ratios are shown in Fig. 4, where they appear nearly identical for the two BPA types. The substantial equivalence already observed under a harmonic force input in Fig. 2 (e) is therefore confirmed under a white-noise force input. Expectedly, the absorber results more effective in H_∞ terms than against a white-noise input (i.e. in H_2 terms).
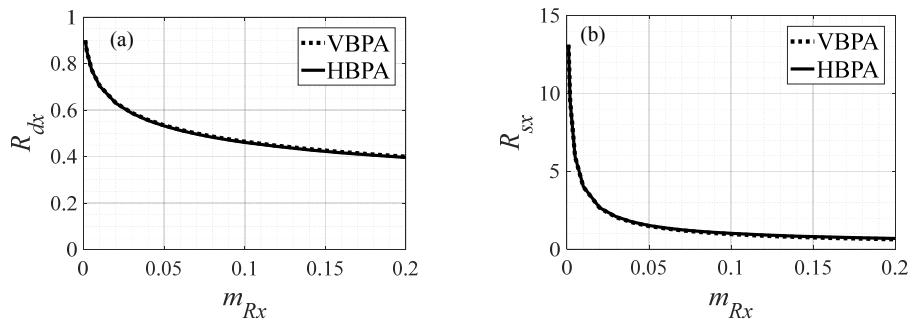

Figure 4: 2D first-order model. VBPA and HBPA response ratios under a unidirectional white-noise force input.

4.2 Natural seismic records

Optimized according to the seismic-oriented design procedure, the evaluation of the VBPA and the HBPA under a white-noise ground acceleration $\ddot{u}_g$ leads to very similar results to those presented in Fig. 4, which are therefore neglected here for brevity.

More interestingly, the structure (with or without BPA) is here subjected to an ensemble of 338 near-field real seismic records, and its period T_{sx} is varied from 0.1 s to 6.0 s, to obtain uncontrolled and controlled spectra. For each interesting response quantity, i.e. the maximum structural displacement $u_{s,max}$ and the maximum BPA stroke u_{max}, the 338 spectra are condensed into their rms spectrum. Dividing, at each period, the controlled rms response spectra by the uncontrolled structural displacement response spectrum, two rms response ratio spectra are obtained, respectively expressed in terms of structural displacement (R_{dx} = rms($u_{s,max}$)con/ rms($u_{s,max}$)unc), and of BPA stroke (R_{sx} = rms(u_{max})con/ rms($u_{s,max}$)unc). Results are presented in Fig. 5 for three mass ratios (m_{Rx} = 1%, 3% and 10%). Again, the VBPA and the HBPA exhibit very similar performances, both in terms of structural displacement and absorber strokes.

5 THREE-DIMENSIONAL SIMULATIONS OF THE FIRST-ORDER MODEL

This section broadens the analysis to 3D models, still operating at low amplitudes, according to (14). The equations of motion are still linear and uncoupled for the VBPA but nonlinear and coupled for the HBPA. The structure is a 2%-damped system having 1 DOF in each direction.
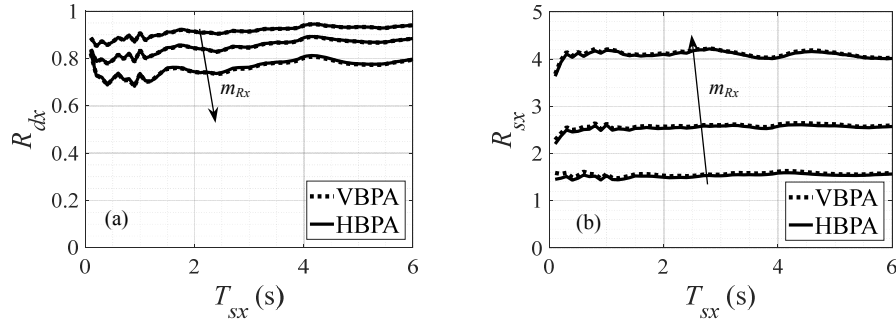
Figure 5: 2D first-order model. VBPA and HBPA response ratio spectra under a unidirectional seismic input, for m_{Rx} = 1%, 3%, 10%.

5.1 White noise force excitation

The structure, with T_{sx} = 1 s and T_{sy}/T_{sx} varying from 1 (axial-symmetry) to 2, is excited by two independent white-noise force input components f_{sx} and f_{sy}, having the same rms value f_{sx0} = f_{sy0}. The mass ratio $m_R = m_{Rx} = m_{Ry}$ is alternatively 1%, 3%, or 10%. The BPA performance is evaluated by considering the average response to 100 realizations of the input process, each one lasting 600 s with a sampling time of 0.01 s. The performance is expressed by the following two bidirectional response ratios: $R_d = \sqrt{R_{dx}R_{dy}}$ and $R_s = \sqrt{R_{sx}R_{sy}}$, which extend to 3D the 2D response ratios introduced in Section 4.1.

Results are shown in Fig. 6, where R_d and R_s are plotted as a function of T_{sy}/T_{sx}. The VBPA performance appears constant with T_{sy}/T_{sx}. The HBPA performance appears approximately constant with T_{sy}/T_{sx}, and quite similar to the VBPA performance, with only slightly larger structural displacements and moderately smaller BPA strokes.
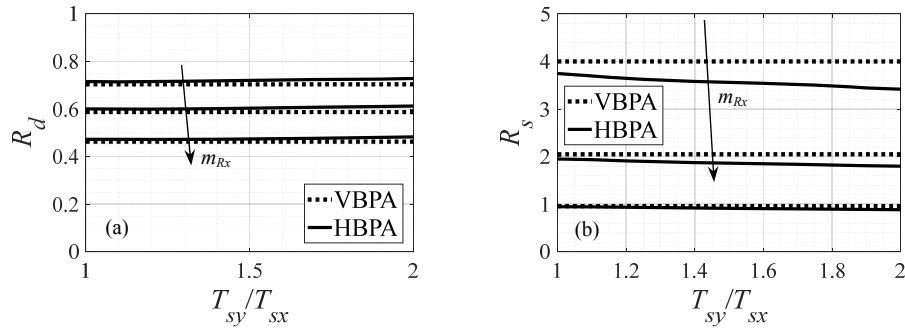

Figure 6: 3D first-order model under a bidirectional white-noise force input. VBPA and HBPA response ratios as a function of T_{sy}/T_{sx}, for m_{Rx} = 1%, 3%, 10%.

5.2 Natural seismic records

The bidirectional performance of the VBPA and of the HBPA is here assessed adopting the same ensemble of seismic records used in Section 4.2. Spectra are computed in terms of 3D rms response ratios, obtained by averaging the corresponding 2D rms response ratios along x and y, according to: $R_d = \sqrt{R_{dx}R_{dy}}$ and $R_s = \sqrt{R_{sx}R_{sy}}$. Fig. 7 shows R_d and R_s evaluated under the assumption that T_{sy}/T_{sx} = 1, for $T_{sx} = T_{sy}$ ranging from 0.5 to 4.0 s, and for m_R alternatively 1%, 3%, or 10%. As in Fig. 6, it appears that under bidirectional excitation, because of friction coupling, the nearly perfect coincidence between the VBPA and the HBPA response is lost. Friction damping implies a slightly larger structural response, and a slightly smaller stroke. The extent of this reduction is however quite limited.
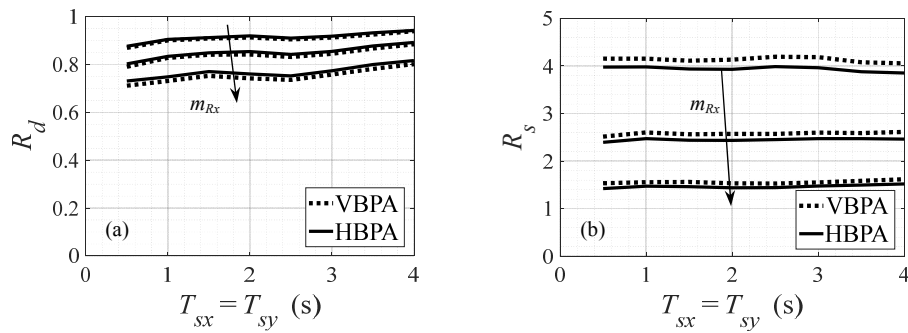
Figure 7: 3D first-order model. VBPA and HBPA response ratio spectra under a bidirectional seismic input, for $T_{sy}/T_{sx} = 1$ and $m_{Rx} = 1\%$, 3%, 10%.

6 TWO-DIMENSIONAL SIMULATIONS OF THE FULLY NONLINEAR MODEL

To show the influence of the excitation intensity on the BPA performance, the optimal VBPA and the optimal HBPA are here compared in the large-displacement domain, by assuming fully nonlinear 2D models. The structure is once again a 2% damped SDOF system.

6.1 White noise force excitation

A structure controlled through a wind-optimal BPA having $m_{Rx} = 3\%$ is simulated under a unidirectional white-noise force input of rms amplitude $\bar{f}_{sx0}$, duration 600 s and sampling time 0.01 s. The response ratios R_{dx} and R_{sx} are shown in Fig. 8 for the two types of BPA as a function of $\bar{f}_{sx0}$ ranging from 0 to 5 N/kg.

For $\bar{f}_{sx0} = 0$, the results are those already obtained in Fig. 4 for first-order models. As $\bar{f}_{sx0}$ increases, the effectiveness in mitigating the structural displacement diminishes, as typical of pendulum devices, and the absorber stroke decreases, as a result of bumping and loss of tuning. The effectiveness reduction appears delayed for the HBPA with respect to the VBPA, because of its amplitude-increasing dissipation capabilities.
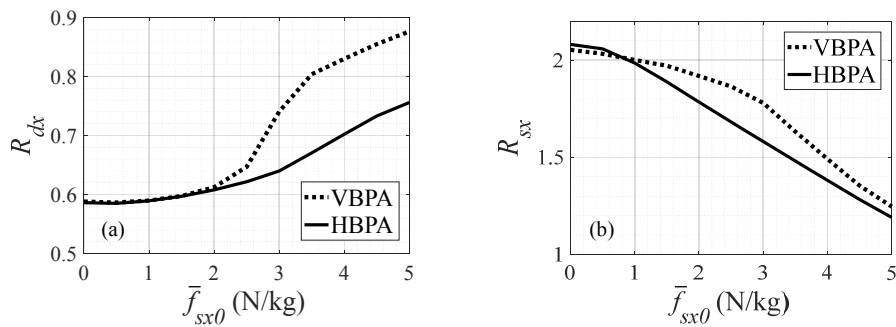

Figure 8: 2D fully nonlinear model. VBPA and HBPA response ratios under a unidirectional white-noise force input, as a function of the input level and for $m_{Rx} = 3\%$.

6.2 Natural seismic records

A structure controlled through a seismic-optimal BPA having $m_{Rx} = 3\%$ is simulated under the ensemble of real records already used in previous sections, for increasing seismic intensities. Denoting by I the intensity ratio, i.e. the dimensionless factor adopted to scale the entire ensemble of records, Fig. 9 reports R_{dx} and R_{sx} as a function of I, for the two BPA types and

for two possible periods of the structure, namely $T_{sx} = 0.5$ s (top subfigures) and $T_{sx} = 4.0$ s (bottom subfigures).

For $I = 0$, the results are those already obtained in Fig. 5 for first-order models. As I increases, both R_{dx} and R_{sx} decrease, as already observed in Section 6.1 under force excitation. However, significant variations are solely observed for $T_{sx} = 0.5$ s, because of the limited stroke capacity of small-period pendulums. In this case, the HBPA appears again superior to the VBPA, because of the increasing damping provided by the proposed friction pattern.
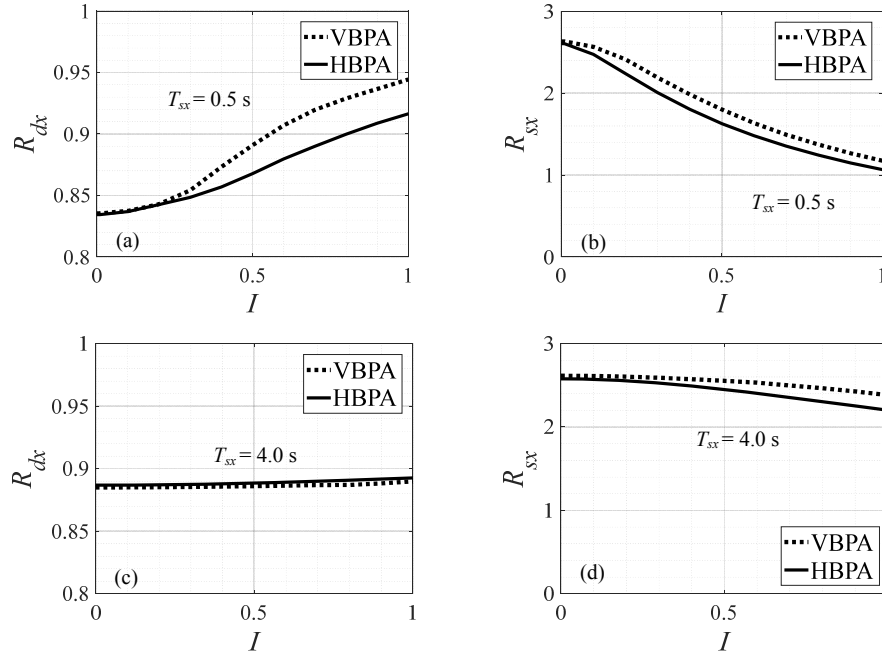

Figure 9: 2D fully nonlinear model. VBPA and HBPA response ratio spectra under a unidirectional seismic input, as a function of I and for $m_{Rx} = 3\%$. Top figures: $T_{sx} = 0.5$ s; bottom figures: $T_{sx} = 4.0$ s.

7 THREE-DIMENSIONAL SIMULATIONS OF THE FULLY NONLINEAR MODEL

7.1 White noise force excitation

The optimal BPAs are mounted on a 2%-damped structure having 1 DOF in each direction, with $T_{sx} = T_{sy} = 1$ s. The structure is excited by a bidirectional white-noise force input, having identical rms amplitude in the two directions, $\bar{f}_{sx0} = \bar{f}_{sy0}$, duration of 600 s, and sampling time of 0.01 s. Simulations are conducted for $\bar{f}_{sx0} = \bar{f}_{sy0}$ ranging from 0 to 5 N/kg, and results are shown in Fig. 10. The performance loss trends already observed for a unidirectional input in Fig. 8 are confirmed. Again, the HBPA performance is similar to the VBPA performance at low intensities, and better for large ones.

7.2 Natural seismic records

Table 1 reports the response ratios obtained by subjecting the controlled structure to the bidirectional seismic records included in the selected ensemble, for $m_R = 3\%$ and for the intensity ratio increasing from 0 to 0.5 to 1.0. Two cases are considered, with the first structural period T_{sx} being fixed at 1.0 s and the second structural period T_{sy} equaling either 1.0 s or 1.5 s. Table 1 confirms that under a bidirectional shaking the VBPA is preferable if second-order effects are negligible ($I = 0$), and the HBPA is preferable if they are not.
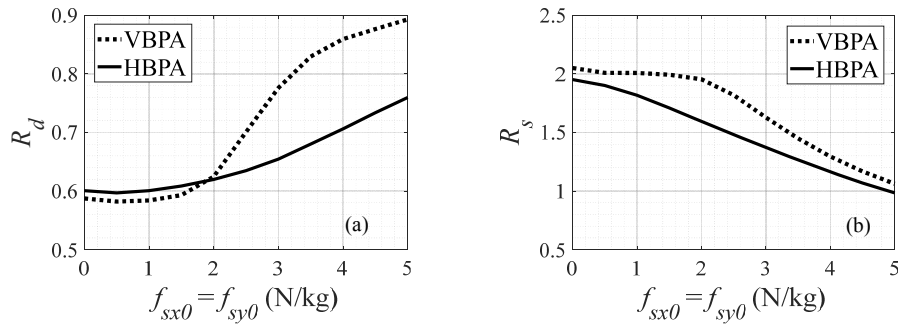
Figure 10: 3D fully nonlinear model. VBPA and HBPA response ratios under a bidirectional white-noise force input, as a function of the input level and for $m_{Rx} = 3\%$. $T_{sx} = T_{sy} = 1.0$ s.

		R_d		R_s	
	I	VBPA	HBPA	VBPA	HBPA
$T_{sx} = 1.0$ s $T_{sy} = 1.0$ s	0.0	0.83	0.84	2.60	2.47
	0.5	0.90	0.88	1.81	1.52
	1.0	0.95	0.92	1.16	1.00
$T_{sx} = 1.0$ s $T_{sy} = 1.5$ s	0.0	0.84	0.85	2.58	2.35
	0.5	0.88	0.87	2.00	1.64
	1.0	0.94	0.91	1.38	1.15

Table 1: 3D fully nonlinear model under seismic input. RMS response ratios for different periods and intensities ($m_R = 3\%$).

8   CASE STUDY: MDOF BUILDING UNDER WIND LOAD

An MDOF high-rise building structure subjected to wind loads is here simulated with or without a BPA atop, using the fully nonlinear model expressed by Eq. (10). The BPA is either of the VBPA or of the HBPA type, in both cases optimized according to the wind-oriented design procedure exposed in Section 3.

The structure is 168 m tall, with a 25 m x 25 m square section. Its shape, mass and stiffness are drawn from [20], but scaled to augment the building sensitivity to the across-wind component. Modelled as a 10-elements cantilever beam, the structure has a flexural stiffness which in the y direction is 1.21 times smaller than in the x direction. The natural periods along y are thus 1.10 times larger than along x. Along x, the first three periods are 4.00 s, 1.23 s, and 0.52 s, with participating modal masses of 45.3%, 21.8%, and 11.1%. Damping is 2% in every mode.

The BPA mass is 1% the total building mass, corresponding to an effective mass ratio of 6.45% according to Warburton [1]. By applying the design procedure presented in Section 3, the VBPA and the HBPA parameters are exposed in Table 2.

	ω_R	ς	μ_0	L_x	L_y	b_x	b_y	b_z	l_{c0}	w_r
	(-)	(-)	(-)	(m)	(m)	(m)	(m)	(m)	(m)	(m)
VBPA	0.93	0.15	-	4.57	5.53	4.79	5.27	5.03	5.03	2.51
HBPA	0.98	-	0.45	4.12	4.99	4.32	4.76	4.53	-	2.27

Table 2: BPA design parameters on the tall building.

Simulations are conducted under a moderate-to-high wind flow, blowing for 1 hour either along x or along y. Deterministic wind load time-histories are determined as the realization of a stationary, spatially nonhomogeneous, stochastic process, comprising both along-wind and across-wind components, acting simultaneously on the structure. Along- and across-wind components are derived according to classical wind load spectra ([21], [22]).

Results are presented in Table 3 only for the wind blowing in the x direction. Four cases are compared, corresponding to: (1) the uncontrolled structure; (2) the linear VBPA; (3) the (geometrically nonlinear) VBPA; and (4) the HBPA. For each case, several response quantities are investigated, including: (i) the maximum modulus of the top story displacement, $r_{N,max}$; (ii) the maximum modulus of the BPA stroke, r_{max}; (iii) the maximum friction damping ratio activated by the HBPA, μ_{max}; (iv) the rms of the modulus of the top story displacement, $r_{N,rms}$; (v) the rms of the modulus of the BPA stroke, r_{rms}; and the mean value of the instantaneous power dissipated by the structure, $W_{s,mean}$.

Case	$r_{N,max}$ (cm)	r_{max} (cm)	μ_{max} (-)	$r_{N,rms}$ (cm)	r_{rms} (cm)	$W_{s,mean}$ (kW)
Uncontrolled	79.4	0.0	-	27.3	0.0	31.1
Linear VBPA	39.6	110	-	13.7	37.5	8.12
VBPA	39.7	109	-	13.8	37.4	8.17
HBPA	38.4	107	0.10	13.7	37.8	8.63

Table 3: Building responses for wind blowing along x.

Table 3 reveals that:
1) With respect to the uncontrolled structure, the linear VBPA achieves a significant response reduction: 50% in $r_{N,max}$ and in $r_{N,rms}$, and 74% in $W_{s,mean}$.
2) The VBPA, accounting for geometrical nonlinearities, gives nearly identical results. The absorber strokes are relatively small and the restrainer is far from being activated, which makes the first-order model accurate enough.
3) The HBPA performance is also very similar to the VBPA performance. The greatest differences are in $W_{s,mean}$, which is 6% larger for the HBPA, and in $r_{N,max}$, which is 3% larger for the VBPA. The maximum friction coefficient met by the HBPA during motion is 0.10.
It can be concluded that the three controlled cases are substantially equivalent.

9   CONCLUSION

Main conclusions of this study can be formulated as follows:
1) The HBPA is shown to be roughly equivalent to the VBPA, especially when responding to a unidirectional excitation at low response amplitudes.
2) Both BPA types undergo a performance loss if the stroke demand exceeds their stroke capacity, as it often occurs in rigid structures under large input intensities. This drawback is partially compensated for the HBPA by its larger dissipation capacity at large displacements. Despite such loss, in all examined simulations both types still ensure a significant vibration mitigation effect.

REFERENCES

[1] G. B. Warburton, Optimum absorber parameters for various combinations of response and excitation parameters, *Earth. Eng. Struct. Dyn.*, **10**, 381-401, 1982.

[2] D. Wang, T.K.T. Tse, Y. Zhou, Q. Li, Structural performance and cost analysis of wind-induced vibration control schemes for a real super-tall building, *Struct. Infrastruct. Eng.*, **11**(8), 990-1011, 2015.

[3] E. Matta, Seismic effectiveness of tuned mass dampers in a life-cycle cost perspective, *Earthq. Struct.*, **9**(1), 73-91, 2015.

[4] R. Greco, G.C. Marano, A. Fiore, Performance-cost optimization of tuned mass damper under low-moderate seismic actions, *Struct. Des. Tall Spec. Build.*, **25**(18), 1103-1122, 2016.

[5] E. Matta, Lifecycle cost optimization of tuned mass dampers for the seismic improvement of inelastic structures, *Earthq. Eng. Struct. Dyn.*, **47**, 714‑737, 2017.

[6] J. Náprstek, C. Fischer, M. Pirner, and O. Fischer, Non-linear model of a ball vibration absorber, *Comput. Meth. Applied Sciences*, **30**, 381-396, 2013.

[7] V. P. Legeza, Rolling of a heavy ball in a spherical recess of a translationally moving body, *Int. Appl. Mech.*, **38**(6), 758-764, 2002.

[8] M. Bransch, Unbalanced oil filled sphere as rolling pendulum on a flat surface to damp horizontal structural vibrations, *J. Sound Vibr.*, **368**, 22-35, 2016.

[9] J. Chen, and C. T. Georgakis, Tuned rolling-ball dampers for vibration control in wind turbines, *J. Sound Vibr.*, **332**, 5271-5282, 2013.

[10] X. Lu, Z. Liu, Z. Lu, Optimization design and experimental verification of track nonlinear energy sink for vibration control under seismic excitation, *Struct. Control Health Monit.*, **24**(12), e2033, 2017.

[11] E. Matta, A. De Stefano, and B. F. Spencer Jr, A new passive rolling-pendulum vibration absorber using a non-axial-symmetrical guide to achieve bidirectional tuning, *Earthq. Eng. Struct. Dyn.*, **38**, 1729-1750, 2009.

[12] J. L. Almazan, J. C. De la Llera, J. A. Inaudi, D. Lopez-Garcia, and L. E. Izquierdo. A Bidirectional and homogeneous tuned mass damper: a new device for passive control of vibrations, *Eng. Struct.*, **29**, 1548-1560, 2007.

[13] E. Matta, A novel bidirectional pendulum tuned mass damper using variable homogeneous friction to achieve amplitude-independent control, *Earthquake Engng. Struct. Dyn.* 2019, 1-25, https://doi.org/10.1002/eqe.3153.

[14] E. Matta, Modeling and design of bidirectional pendulum tuned mass dampers using axial or tangential homogeneous friction damping, *Mech. Syst. Signal Proc. 116*, 392-414, 2019.

[15] J. Inaudi, and J. Kelly, Mass damper using friction-dissipating devices, *J. Eng. Mech.*, **121**, 142-149, 1995.

[16] A. Fiore, G.C. Marano, M.N. Natale, Theoretical prediction of the dynamic behavior of rolling-ball rubber-layer isolation systems, *Struct. Control Health. Monit.*, **23**, 1150‑1167, 2016.

[17] R. Greco, G.C. Marano, Identification of parameters of Maxwell and Kelvin-Voigt generalized models for fluid viscous dampers, *J. Vibr. Control*, **21**(2), 260–274, 2015.

[18] J. B. Burl, *Linear Optimal Control*. Menlo Park, CA: Addison-Wesley, Longman, 1999.

[19] A. Y. T. Leung, and H. Zhang, Particle swarm optimization of tuned mass dampers, *Eng. Struct.*, **31**, 715-728, 2009.

[20] Y. L. Xu, B. Samali, and K. C. S. Kwok, Control of along-wind response of structures by mass and liquid dampers, *J. Eng. Mech.*, 118(1), 20-39, 1992.

[21] A. G. Davenport, The spectrum of horizontal gustiness near the ground in high winds, *Q. J. R. Meteorol. Soc.*, **87**, 194-211, 1961.

[22] B. J. Vickery, and A. W. Clarke, Lift or across-wind response of tapered stacks, *J. Struct. Div. ASCE*, **98**, 1-20, 1972.